CF+ excitation in the interstellar medium

Benjamin Desrousseaux, François Lique, Javier R. Goicoechea, Ernesto Quintas-Sánchez, Richard Dawes

A&A 645, A8 (2021)
https://doi.org/10.1051/0004-6361/202039823

Astronomy & Astrophysics

CF^+ excitation in the interstellar medium

Benjamin Desrousseaux[1], François Lique[1], Javier R. Goicoechea[2], Ernesto Quintas-Sánchez[3], and Richard Dawes[3]

[1] LOMC – UMR 6294, CNRS-Université du Havre, 25 rue Philippe Lebon, BP 1123, 76063 Le Havre Cedex, France
e-mail: benjamin.desrousseaux@univ-lehavre.fr
[2] Instituto de Física Fundamental (CSIC). Calle Serrano 121-123, 28006 Madrid, Spain
[3] Department of Chemistry, Missouri University of Science and Technology, Rolla, Missouri 65409, USA

Received 1 November 2020 / Accepted 24 November 2020

ABSTRACT

The detection of CF^+ in interstellar clouds potentially allows astronomers to infer the elemental fluorine abundance and the ionization fraction in ultraviolet-illuminated molecular gas. Because local thermodynamic equilibrium (LTE) conditions are hardly fulfilled in the interstellar medium (ISM), the accurate determination of the CF^+ abundance requires one to model its non-LTE excitation via both radiative and collisional processes. Here, we report quantum calculations of rate coefficients for the rotational excitation of CF^+ in collisions with para- and ortho-H_2 (for temperatures up to 150 K). As an application, we present non-LTE excitation models that reveal population inversion in physical conditions typical of ISM photodissociation regions (PDRs). We successfully applied these models to fit the CF^+ emission lines previously observed toward the Orion Bar and Horsehead PDRs. The radiative transfer models achieved with these new rate coefficients allow the use of CF^+ as a powerful probe to study molecular clouds exposed to strong stellar radiation fields.

Key words. ISM: general – masers – scattering – molecular data – radiative transfer

1. Introduction

Although fluorine is one of the most reactive species in the interstellar medium (ISM; Neufeld et al. 2005; Neufeld & Wolfire 2009), the chemistry of the most abundant F-bearing molecules, HF and CF^+, can be accurately described by a few chemical reactions that depend on the amount of F atoms, H_2 molecules, and C^+ ions (Neufeld et al. 2005). CF^+ is produced in ISM regions bathed by stellar ultraviolet (UV) photons able to ionize carbon atoms in diffuse interstellar clouds or at the illuminated surfaces of dense molecular clouds (so-called photodissociation regions; PDRs). The simplicity of the fluorine chemical network results in a great sensitivity of astrophysical models to molecular data (reactive rate coefficients).

Interstellar CF^+ was first detected in the Orion Bar PDR by Neufeld et al. (2006). Since then, this molecular ion has been widely observed in other PDRs and diffuse clouds of the Milky Way and beyond (Neufeld et al. 2006; Kalenskii & Johansson 2010a,b; Guzmán et al. 2012a; Liszt et al. 2014, 2015; Muller et al. 2016; Nagy et al. 2013, 2017). In these environments, the CF^+ abundance is a powerful proxy for C^+ (closely related to the ionization fraction) and for F atoms, which are both difficult to observe (Guzmán et al. 2012a). Because local thermodynamic equilibrium (LTE) conditions are hardly fulfilled in the ISM (Roueff & Lique 2013), the competition between radiative and collisional processes has to be taken into account in the molecular line modeling in order to derive an accurate CF^+ abundance and gas physical conditions. Collisional data for collisions between CF^+ and the most abundant species in the ISM (usually atomic and molecular hydrogen) are then essential. Collisional rate coefficients with He, as a template for H_2, were first computed by Ajili & Hammami (2013) and recently updated by Denis-Alpizar et al. (2018). However, it is well established (Roueff & Lique 2013) that He data are a bad surrogate for H_2 in case of collisions with an ion.

Denis-Alpizar & Rubayo-Soneira (2019) provided the first proper study of the CF^+–H_2 system. They treated the rotational relaxation of CF^+ by para-H_2 using a reduced-dimensional potential energy surface (PES) averaged over H_2 rotation. The use of an averaged PES, however, only allows one to consider collisions of CF^+ with a spherical H_2, neglecting anisotropy effects due to the H_2 rotation.

CF^+ is mostly detected in warm molecular gas, where the H_2 ortho-to-para ratio is found to be large, therefore obtaining rate coefficients for collisional excitation with ortho-H_2 is crucial and cannot be achieved considering a spherical structure-less H_2.

In order to overcome this limitation, Desrousseaux et al. (2019) recently presented a new highly accurate four-dimensional (4D) PES, by which the calculation of rate coefficients for collisional excitation of CF^+ by both para- and ortho-H_2 is made possible. In that work, preliminary cross-sections at low collisional energy (up to 150 cm^{-1}) were presented for both para- and ortho-H_2 collisions. In this paper, we describe further results using this recently computed CF^+–H_2 4D PES (Desrousseaux et al. 2019) to carry out scattering calculations of rate coefficients for the collisional excitation of CF^+ by H_2. We also used the new collisional data to simulate the excitation of CF^+ in the ISM. We demonstrate that CF^+ exhibits population inversion at typical physical conditions of molecular clouds, and we show that CF^+ is a powerful tracer of the gas characteristics in diffuse interstellar clouds and illuminated surfaces of dense molecular clouds.

The CF^+-H_2 PES was computed employing electronic structure data from coupled-cluster theory extrapolated to the complete basis set (CBS) limit and constructed using the recently

released software-package AUTOSURF (Quintas-Sánchez & Dawes 2019). On this PES, a global minimum of −1230.2 cm^{-1} is found for a planar structure with the two monomers almost parallel (see Desrousseaux et al. 2019 for more details). This large energy well-depth, typical for ion-molecule collisional systems, makes employing state-of-the-art methods to compute the cross-sections very challenging, and, to the best of our knowledge, only four molecular ions (CN^- Kłos & Lique 2011, HCO^+ Massó & Wiesenfeld 2014, C_6H^- Walker et al. 2016, and SH^+ Dagdigian 2019b,a) among the 38 detected in the ISM have been studied in collision with nonspherical H_2.

2. Scattering calculations

The MOLSCAT nonreactive scattering code (Hutson & Green 2012) was used to carry out close-coupling calculations of the rotational (de)excitation cross-sections for collisions between CF^+ and both para- and ortho-H_2. The cross-sections were computed using the quantum time-independent close-coupling (CC) approach and the hybrid log-derivative/Airy propagator implemented in the MOLSCAT code. In the following, molecule-related parameters are labeled with subscripts 1 and 2, referring to the CF^+ and H_2 molecules, respectively.

The expansion over angular functions of the potential was performed as described by Green (1975):

$$V(R,\theta_1,\theta_2,\varphi) = \sum_{l_1,l_2,l} v_{l_1,l_2,l}(R) A_{l_1,l_2,l}(\theta_1,\theta_2,\varphi), \quad (1)$$

where $A_{l_1,l_2,l}(\theta_1,\theta_2,\varphi)$ is constructed from coupled spherical functions $Y_{l_i,m_i}(\theta_i,\varphi)$ and the rotational angular momenta of CF^+ and H_2. The potential was expanded including $0 \le l_1 \le 24$ for the CF^+ molecule, and $0 \le l_2 \le 6$ for the H_2 molecule.

The two molecules were considered as rigid rotors. The molecular constants of CF^+ were set at the value given by Cazzoli et al. (2010): $B_e = 1.720912$ cm^{-1}, $\alpha_e = 0.0189$ cm^{-1}, and $D_e = 63 \times 10^{-6}$ cm^{-1}. The molecular constants of H_2 were set as (Herzberg & Huber 1979) $B_e = 60.853$ cm^{-1}, $\alpha_e = 3.062$ cm^{-1}, and $D_e = 4.71 \times 10^{-2}$ cm^{-1}.

Cross-sections were obtained for the first 22 rotational levels of CF^+ ($0 \le j_1 \le 21$). As already discussed in Desrousseaux et al. (2019), convergence of these cross-sections was ensured by including the 33 lowest rotational levels of CF^+ and only the lowest rotational levels of para-H_2 ($j_2 = 0$) and ortho-H_2 ($j_2 = 1$) in the basis set.

At each collisional energy, the maximum value of the total angular momentum J_{tot} was automatically determined by the MOLSCAT code in order to converge cross-sections to better than 1×10^{-4} Å^2, going up to $J_{tot} = 120$ at the highest energies.

The determination of the thermal rate coefficients was achieved by averaging the cross-sections $\sigma_{\alpha\to\beta}$ over the collisional energy (E_c):

$$k_{\alpha\to\beta}(T) = \left(\frac{8}{\pi\mu k_B^3 T^3}\right)^{\frac{1}{2}} \times \int_0^\infty \sigma_{\alpha\to\beta}\, E_{ce}^{-\frac{E_c}{k_B T}}\, dE_c, \quad (2)$$

where μ is the reduced mass of the colliding system and k_B is the Boltzmann's constant. α and β, respectively, designate the initial and final rotational states of the CF^+ molecule. Collisional energies up to 1500 cm^{-1} were explored in order to allow the determination of the rate coefficients for collisions between CF^+ and both para- and ortho-H_2 up to 150 K for the first 22 rotational levels of CF^+.

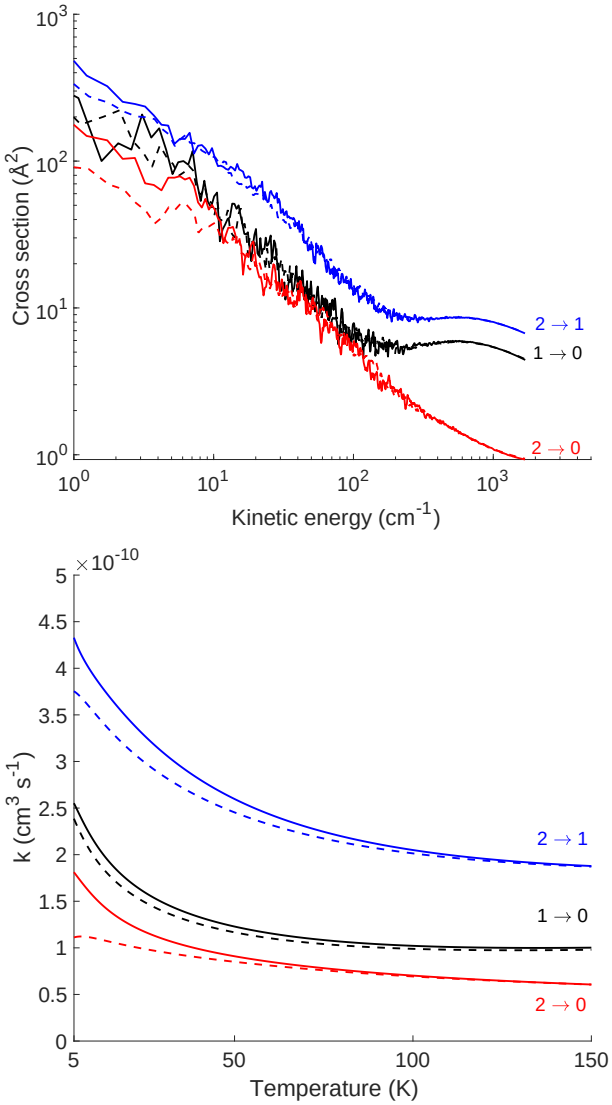

Fig. 1. Cross-sections (*upper panel*) and rate coefficients (*lower panel*) for the collisional excitation of CF^+ by para-$H_2(j_2 = 0)$ (solid lines) and ortho-$H_2(j_2 = 1)$ (dashed lines) for selected rotational transitions $j_1 \to j_1'$.

Cross-sections and corresponding rate coefficients for some selected transitions are displayed in Fig. 1. The cross-sections (upper panel) present the same behavior for both para- and ortho-H_2. At low energy (up to a few hundreds cm^{-1}), the cross-sections decrease with increasing energy, following an almost linear dependence as a function of the energy logarithm. This behavior is typical and expected, as predicted from Langevin theory for ion–molecule collisions. The cross-sections also exhibit many resonances in this energy region. This can be explained by the creation of quasi-bound states within the deep van der Waals well of the CF^+–H_2 complex before its dissociation, as already discussed by Denis-Alpizar et al. (2020). At higher energies, it is generally observed that the cross sections are slowly decreasing with increasing energy, beyond a slight initial increase for transitions with low Δj_1. The magnitude of the cross-sections seems to be approximately the same for collisions with either para- or ortho-H_2, except at very low collisional energies (<10 cm^{-1}), where differences of up to a factor of 2 can be seen for large Δj_1 transitions.

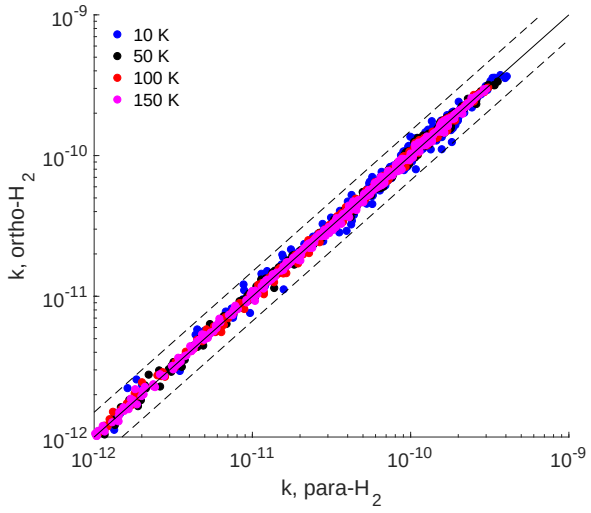

Fig. 2. Comparison between rate coefficients (in units of cm^3 s^{-1}) for the collisional excitation of CF$^+$ by para- and ortho-H_2. Rotational transitions involving the first 22 rotational levels of CF$^+$ are presented at four different temperatures. The two dashed lines delimit the region where the rate coefficients differ by less than a factor of 1.5.

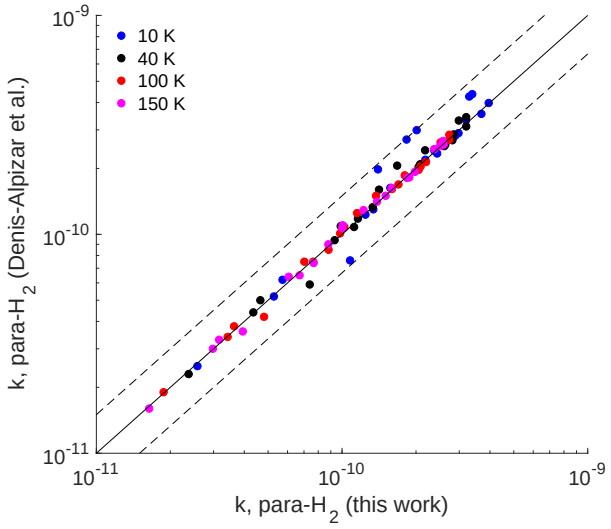

Fig. 3. Comparison between rate coefficients (in units of cm^3 s^{-1}) for the collisional deexcitation of CF$^+$ by para-H_2 obtained in this work and those obtained by Denis-Alpizar & Rubayo-Soneira (2019). Deexcitation transitions involving the first seven rotational levels of CF$^+$ are presented at four different temperatures. The two dashed lines delimit the region where the rate coefficients differ by less than a factor of 1.5.

The corresponding rate coefficients (lower panel) show a relatively flat temperature dependence, as predicted by the Langevin theory. The magnitude of the rate coefficients decreases with increasing Δj_1, with propensity rules in favor of transitions with $\Delta j_1 = 1$. Not surprisingly, given the similar cross-sections, it is also observed that rate coefficients for collisions with para- and ortho-H_2 are similar in magnitude.

This similarity between para- and ortho-H_2 rate coefficients is explored further in Fig. 2, which compares para- and ortho-H_2 collisional rate coefficients for the rotational excitation of CF$^+$ at four different temperatures (10, 50, 100, and 150 K), and for all transitions involving the first 22 rotational levels of CF$^+$. As highlighted by the two dashed lines, differences between the two sets of data are quite small and do not exceed 50%. The agreement improves with increasing temperature, with differences of less than 10% being observed for temperatures above 50 K. It should also be noted that for the most dominant transitions ($k > 2\times10^{10}$ cm^3 s^{-1}), differences stay lower than 10% for all the temperatures explored. This global agreement between para- and ortho-H_2 rate coefficients confirms what has already been observed for a wide variety of ion–molecule collisions (Massó & Wiesenfeld 2014; Walker et al. 2017; Denis-Alpizar et al. 2020; Balança et al. 2020; Kłos & Lique 2011).

In Fig. 3, we present a comparison between rate coefficients for the collisional deexcitation of CF$^+$ by para-H_2 obtained in this work and those obtained by Denis-Alpizar & Rubayo-Soneira (2019). The agreement between the two sets of data is good overall, with differences of less than 10% generally observed at high temperatures (≥40 K). At low temperatures, and, in particular, for the most dominant transitions, differences up to 50% can be seen. These differences can likely be attributed to the different levels of electronic structure calculations used to generate the PESs, as well the use of an averaged version of this PES, neglecting the H_2 structure. Therefore, we recommend the use of our new rate coefficients in astrophysical applications.

3. Excitation and radiative transfer study

In order to test the impact of the new collisional rate coefficients in astrophysical applications, the RADEX (van der Tak et al. 2007) code was used to perform non-LTE radiative transfer calculations[1] using the escape probability formalism, assuming an isothermal and homogeneous medium.

The radiation field value was taken as the cosmic microwave background at 2.73 K, and the line width was set at 1 km s^{-1}. Energy levels, transition frequencies, and Einstein A coefficients were taken from the Cologne Database for Molecular Spectroscopy (CDMS; Müller et al. 2005).

Collisional deexcitation rate coefficients for the first 22 rotational levels of CF$^+$ (231 collisional transitions) obtained in this work were included for temperatures up to 150 K. Note that because of the absence of nuclear spin-dependence of the rate coefficients, we only considered collisional excitation of CF$^+$ through para-H_2 collisions in the calculations.

It should also be noted that electron collisions were not included in these radiative transfer calculations. To the best of our knowledge, there is no available data for the collisional excitation of CF$^+$ by electrons. Nevertheless, while CF$^+$ is detected in regions of high ionization fractions, with the electron density given by $n_e = n_H \times X(C^+) \sim 2n(H_2) \times 10^{-4}$ cm^{-3}, as for many molecular ions, CF$^+$–H_2 collisional rate coefficients are particularly large: $>10^{-10}$ cm^3 s^{-1}. This implies that in order for electronic collisions to contribute to the excitation process of CF$^+$ molecules, electron rate coefficients should be greater than a few 10^{-6} cm^3 s^{-1}, and even greater than 10^{-5} cm^3 s^{-1} to dominate.

The H_2-density variation of the excitation temperatures and population levels were computed for a grid of kinetic temperatures ranging from 10 to 150 K and column densities ranging from 10^7 to 10^{15} cm^{-2}. In Fig. 4, we represent the H_2-density variation of the excitation temperature[2] and the optical depth τ

[1] The collisional rate coefficients are made available as a RADEX datafile in the LAMDA database (Schöier et al. 2005).

[2] $n_u/n_l = g_u/g_l \exp[-E_{ul}/k_B T_{ex}]$, where n_u (n_l) represents the population of the upper (lower) level, g_u (g_l) the degeneracy of the upper (lower) level, E_{ul} the difference of energy between the upper and lower levels, and k_B the Boltzmann constant. $T_{ex} = T_k$ corresponds to LTE conditions.

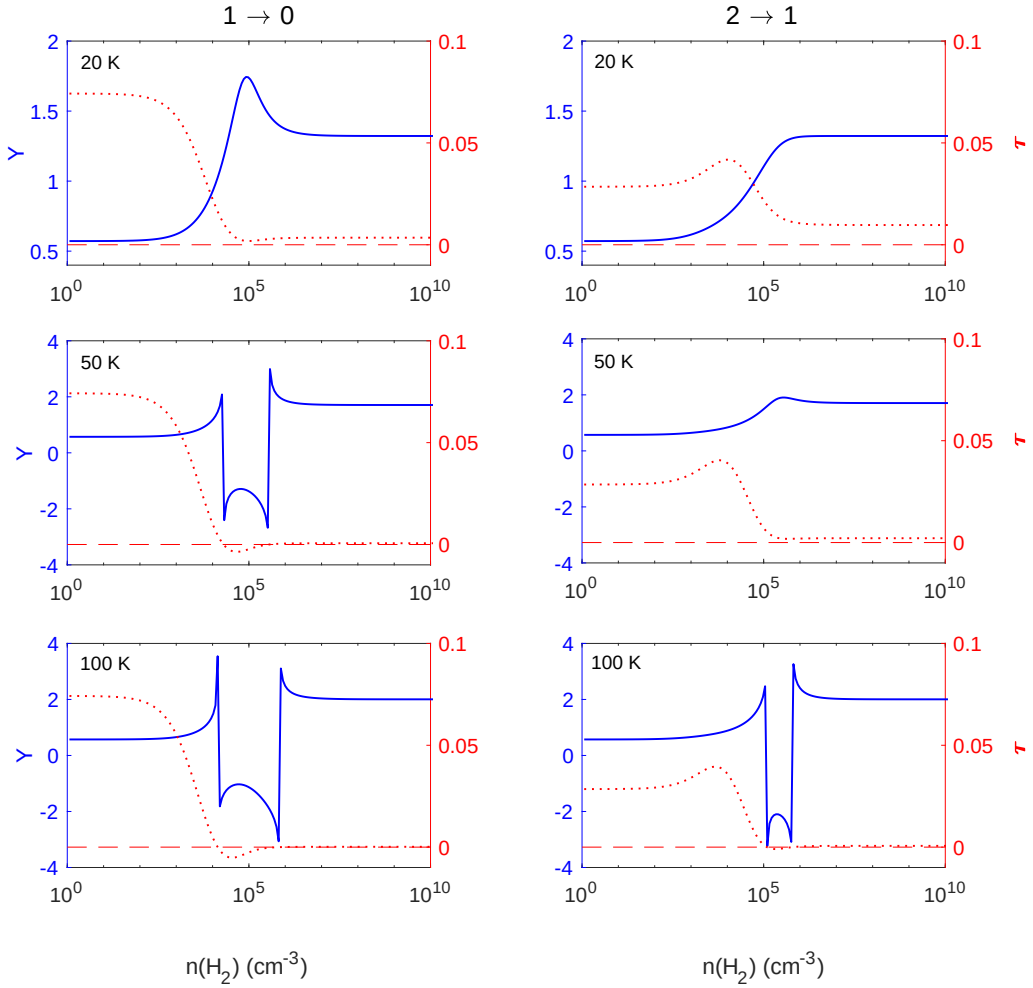

Fig. 4. Variation of excitation temperature (blue solid lines) and optical depth (red dotted lines) as a function of H_2-density for the 1 → 0 (*left panels*) and 2 → 1 (*right panels*) CF^+ rotational transitions at kinetic temperatures of 20 K (*upper panels*), 50 K (*middle panels*), and 100 K (*lower panels*), and a CF^+ column density of $N(CF^+) = 1 \times 10^{12}$ cm^{-2}. In order to better display the large amplitude of its variation, the excitation temperature is represented on this figure as $Y = \frac{T_{ex}}{|T_{ex}|} \times \log_{10}(1 + |T_{ex}|)$.

for the 1 → 0 and 2 → 1 CF^+ rotational lines. We explore kinetic temperatures of 20, 50, and 100 K, and a CF^+ column density of 10^{12} cm^{-2}, corresponding to the typical value inferred from previous observations (Neufeld et al. 2006; Guzmán et al. 2012a; Nagy et al. 2017) in PDRs.

At low temperatures ($T_k = 20$ K), the 1 → 0 rotational line exhibits supra-thermal emission ($T_{ex} > T_k$) in the H_2-density range of ∼10^4–10^6 cm^{-3}. At higher kinetic temperatures (50 and 100 K), the excitation temperature becomes negative in approximately the same H_2-density range. The same behavior is observed for the 2 → 1 line in a narrower H_2-density range and at higher temperatures: supra-thermal excitation appears at ∼50 K in the H_2-density range of ∼10^5–10^6 cm^{-3}, while negative excitation temperatures are observed at a kinetic temperature of 100 K. This negative excitation temperature behavior indicates a level population inversion ($n_u/g_u > n_l/g_l$). However, as can be seen in Fig. 4, at the relatively low CF^+ column densities present in prototypical PDRs, the opacities of the inverted lines remain very low ($-\tau \ll 1$) for all the explored physical conditions. This implies a negligible maser amplification insufficient to exhibit an observable effect.

Finally, we used these RADEX models to infer the H_2 gas density at the UV-illuminated surfaces of the Horsehead and Orion Bar PDRs from the observed CF^+ line emission. In particular, we tried to fit the CF^+ emission spectra reported by Neufeld et al. (2006), Guzmán et al. (2012a,b), and Nagy et al. (2017) summarized in Table 1.

In order to determine the set of parameters (T, $n(H_2)$ and $N(CF^+)$) that best reproduces the observations, we calculated the χ^2-value for each set of parameters as follows:

$$\chi^2 = \sum_{i=1}^{n} \left(\frac{W_i^{obs} - W_i^{calc}}{\sigma_i} \right)^2, \quad (3)$$

where n is the number of observed CF^+ rotational lines, W^{calc} is the integrated line intensity obtained from RADEX simulations, W^{obs} is the observed integrated line intensity reported in the papers, and σ is the uncertainty on the observed value. The best fit is then obtained by minimizing the χ^2 values.

These fits implicitly assume that the observed CF^+ emission is spatially extended (i.e., it fills the beam of the telescope at each observed frequency). This is a reasonable assumption because CF^+ is expected to arise from the extended C^+ layers at the edge of PDRs (see models of Neufeld & Wolfire 2009; Guzmán et al. 2012b).

Table 1. Observed CF^+ integrated line intensities in the Horsehead and Orion Bar PDRs.

		Critical density [a] (10^5 cm^{-3})			W (mK km s^{-1})	
Rotational line	Frenquency (GHz)	20 K	50 K	100 K	Horsehead	Orion Bar
$1 \rightarrow 0$	102.58748	0.28	0.39	0.48	150 ± 20	86 ± 10
$2 \rightarrow 1$	205.17445	1.34	1.78	2.46	290 ± 40	337 ± 13
$3 \rightarrow 2$	307.7443	5.16	5.80	7.04	–	428 ± 34
$5 \rightarrow 4$	512.8465	11.76	13.36	15.07	–	100 ± 20

Notes. [a]Critical density: $n_{cr} = \frac{A_{ij}}{k_{ij}}$, where i and j, respectively, designate the initial and final rotational number, A is the Einstein coefficient, and k is the collisional rate coefficient.
References. Neufeld et al. (2006); Guzmán et al. (2012a); Nagy et al. (2017).

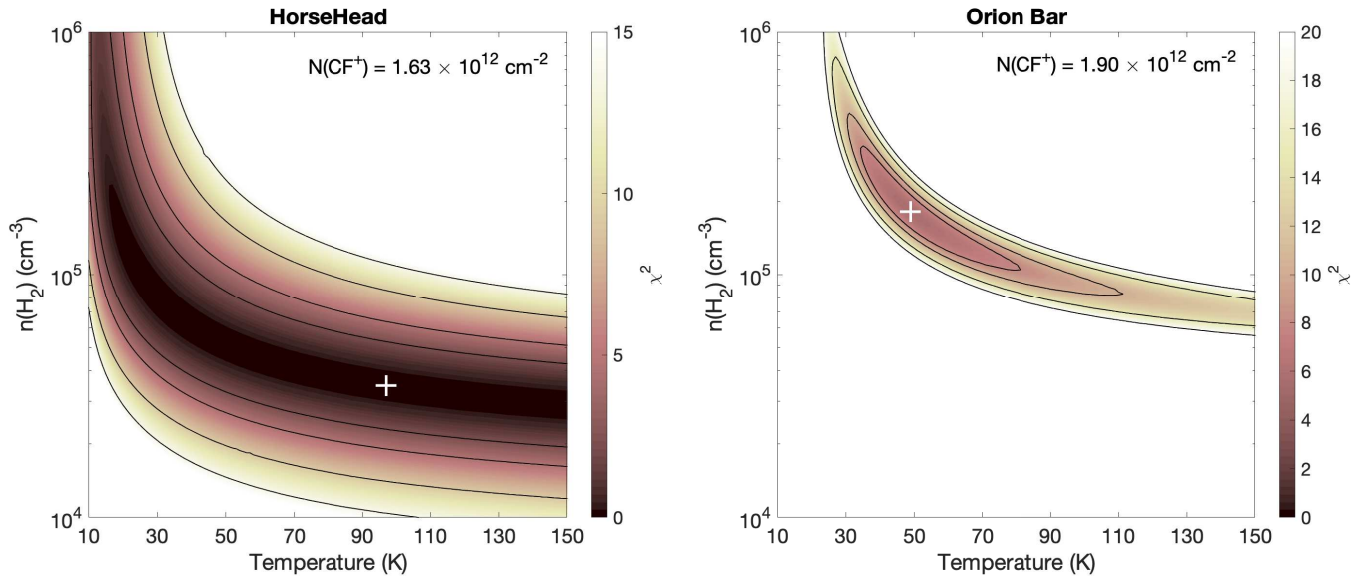

Fig. 5. χ^2-value as a function of the H_2 column density and gas kinetic temperature for the Horsehead (*left panel*) and Orion Bar (*right panel*) PDRs. The solid black lines represent confidence contour levels of 63.3, 90.0, 99.0 and 99.9%. The sets of parameters (T, $n(H_2)$) which give minimum χ^2 are indicated with a white + symbol.

For both sources, the best-fit value for the CF^+ column density $N(CF^+)$ allowing us to reproduce the observed line strengths were 1.63×10^{12} and 1.90×10^{12} cm^{-2} for the Horsehead and Orion Bar regions, respectively. In Fig. 5, we present the χ^2-value as a function of the H_2 gas density and gas kinetic temperature for both Horsehead and Orion Bar PDRs at the corresponding CF^+ column densities. In this figure, we also represent contour levels where the probability of enclosing the correct parameters T, $n(H_2)$ and $N(CF^+)$ is 63.3, 90.0, 99.0, and 99.9%. This is achieved by considering the regions where $\chi^2 \leq \chi^2_{\rm min} + \Delta\chi^2$ for $\Delta\chi^2$ values of 2.3, 4.6, 9.2, and 13.8 (Lampton et al. 1976). The sets of parameters (T, $n(H_2)$) that give minimum χ^2 (i.e., the best fit) are indicated with a white + symbol: we obtain kinetic temperatures of 100 and 50 K, and H_2 gas densities of 3.5×10^4 and 1.8×10^5 cm^{-3}, for the Horsehead and Orion Bar PDRs, respectively.

In those two prototypical PDRs, the gas temperature of the C^+-emitting layers (likely similar to the CF^+-emitting layers at the UV-illuminated cloud surface) are observationally well constrained to $T_k = 60-100$ K in the Horsehead (Pabst et al. 2017) and $T_k = 150-200$ K in the Orion Bar (Goicoechea et al. 2017). We note that a more refined determination of the gas density would require one to spatially resolve the true size of the CF^+-emitting regions (e.g., with ALMA) and carry out PDR-depth dependent excitation models. If we assume that the CF^+ emission in the Orion Bar arises from a 10″-width filament (similar to other molecular ions such as SH^+, Goicoechea et al. 2017) and correct the observed line intensities by the appropriate beam filling factors, we obtain reasonable fits consistent with gas temperatures of about 100 K and H_2 gas density $n(H_2) \sim 7 \times 10^4$ cm^{-3}.

4. Summary

In summary, we computed rate coefficients for inelastic collisions of CF^+ by both para- and ortho-H_2 for temperatures up to 150 K and rotational transitions between the first 22 levels of the CF^+ molecule ($0 \leq j_1 \leq 21$). We used these new rate coefficients in non-LTE excitation and radiative transfer calculations that reveal inversion population and weak maser CF^+ emission at gas physical conditions corresponding to those in regions where this molecule can be observed. Finally, we were able to constrain gas density at the surface of the Horsehead and Orion Bar PDRs by reproducing their observed CF^+ line intensities.

Acknowledgements. F.L. acknowledges financial support from the Institut Universitaire de France. We acknowledge the Programme National Physique et Chimie du Milieu Interstellaire (PCMI) of CNRS/INSU with INC/INP co-funded by CEA and CNES. This work was granted access to the Occigen HPC resources of CINES under the allocation 2019 [A0070411036] made by GENCI. J.R.G.

thanks the Spanish MICIU for funding support under grants AYA2017-85111-P and PID2019-106110GB-I00. R.D. is supported by the US Department of Energy Office of Science, Office of Basic Energy Sciences (Award DE-SC0019740).

References

Ajili, Y., & Hammami, K. 2013, A&A, 556, A82
Balança, C., Scribano, Y., Loreau, J., Lique, F., & Feautrier, N. 2020, MNRAS, 495, 2524
Cazzoli, G., Cludi, L., Puzzarini, C., & Gauss, J. 2010, A&A, 509, A1
Dagdigian, P. J. 2019a, MNRAS, 487, 3427
Dagdigian, P. J. 2019b, J. Chem. Phys., 150, 084308
Denis-Alpizar, O., & Rubayo-Soneira, J. 2019, MNRAS, 486, 1255
Denis-Alpizar, O., Inostroza, N., & Castro Palacio, J. C. 2018, MNRAS, 473, 1438
Denis-Alpizar, O., Stoecklin, T., Dutrey, A., & Guilloteau, S. 2020, MNRAS, 497, 4276
Desrousseaux, B., Quintas-Sánchez, E., Dawes, R., & Lique, F. 2019, J. Phys. Chem. A, 123, 9367
Goicoechea, J. R., Pety, J., Cuadrado, S., et al. 2016, Nature, 537, 207
Goicoechea, J. R., Cuadrado, S., Pety, J., et al. 2017, A&A, 601, L9
Green, S. 1975, J. Chem. Phys., 62, 2271
Guzmán, V., Pety, J., Gratier, P., et al. 2012a, A&A, 543, L1
Guzmán, V., Roueff, E., Gauss, J., et al. 2012b, A&A, 548, A94
Herzberg, G., & Huber, K. P. 1979, Molecular Spectra and Molecular Structure (New York London: Van Nostrand Reinhold)
Hutson, J. M., & Green, S. 2012, Astrophys. Source Code Libr. [record ascl:1206.004]
Kalenskii, S. V., & Johansson, L. E. B. 2010a, Astron. Rep., 54, 295
Kalenskii, S. V., & Johansson, L. E. B. 2010b, Astron. Rep., 54, 1084
Kłos, J., & Lique, F. 2011, MNRAS, 418, 271
Lampton, M., Margon, B., & Bowyer, S. 1976, ApJ, 208, 177
Liszt, H. S., Pety, J., Gerin, M., & Lucas, R. 2014, A&A, 564, A64
Liszt, H. S., Guzmán, V. V., Pety, J., et al. 2015, A&A, 579, A12
Massó, H., & Wiesenfeld, L. 2014, J. Chem. Phys., 141, 184301
Müller, H. S., Schlöder, F., Stutzki, J., & Winnewisser, G. 2005, J. Mol. Struct., 742, 215
Muller, S., Kawaguchi, K., Black, J. H., & Amano, T. 2016, A&A, 589, L5
Nagy, Z., Van der Tak, F. F. S., Ossenkopf, V., et al. 2013, A&A, 550, A96
Nagy, Z., Choi, Y., Ossenkopf-Okada, V., et al. 2017, A&A, 599, A22
Neufeld, D. A., & Wolfire, M. G. 2009, ApJ, 706, 1594
Neufeld, D. A., Wolfire, M. G., & Schilke, P. 2005, ApJ, 628, 260
Neufeld, D. A., Schilke, P., Menten, K. M., et al. 2006, A&A, 454, L37
Pabst, C. H. M., Goicoechea, J. R., Teyssier, D., et al. 2017, A&A, 606, A29
Quintas-Sánchez, E., & Dawes, R. 2019, J. Chem. Inf. Model., 59, 262
Roueff, E., & Lique, F. 2013, Chem. Rev., 113, 8906
Schöier, F. L., van der Tak, F. F. S., van Dishoeck, E. F., & Black, J. H. 2005, A&A, 432, 369
van der Tak, F., Black, J., Schoeier, F., Jansen, D., & van Dishoeck, E. 2007, A&A, 468, 627
Walker, K. M., Dumouchel, F., Lique, F., & Dawes, R. 2016, J. Chem. Phys., 145, 024314
Walker, K. M., Lique, F., Dumouchel, F., & Dawes, R. 2017, MNRAS, 466, 831